# Nanoscale

Accepted Manuscript


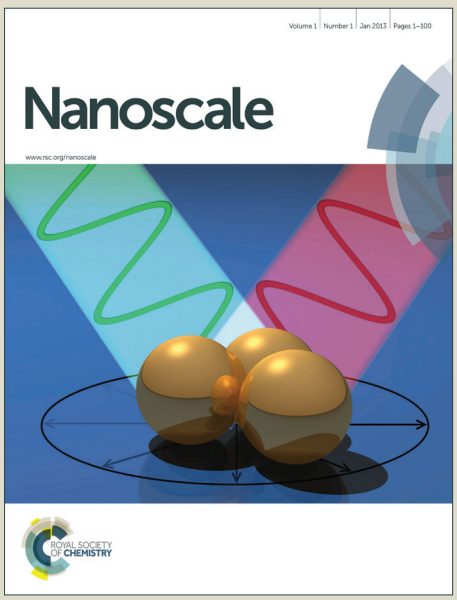





ROYAL SOCIETY OF CHEMISTRY

www.rsc.org/nanoscale

Journal Name

RSCPublishing

ARTICLE

# Effect of trimetallization in thiolate-protected $Au_{24-n}Cu_nPd$ clusters

Cite this: DOI: 10.1039/x0xx00000x

Sachil Sharma,[a] Wataru Kurashige,[a] Katsuyuki Nobusada[b,c] and Yuichi Negishi*[a,d,e]

Received 00th January 2012,
Accepted 00th January 2012

DOI: 10.1039/x0xx00000x

www.rsc.org/

We synthesized a mixture of $Au_{24-n}Cu_nPd(SC_{12}H_{25})_{18}$ ($n$ = 0-3) and $Au_{25-n}Cu_n(SC_{12}H_{25})_{18}$ ($n$ = 0-7) and compared their stability. The results showed that, in a cluster containing one Cu atom, the presence of Pd is effective in improving the cluster stability. Conversely, the presence of Pd has different effects depending on the number of Cu atoms in the cluster: cluster formation was inhibited for clusters containing four or more Cu atoms.

## Introduction

Intermetallic compound clusters comprising two types of elements exhibit different physical and chemical properties than monometal counterparts. For example, the catalytic activity of polymer-stabilized $Pd_{147}$ clusters is remarkably improved when the Pd at the surface is partially substituted by Au.[1] In addition, intermetallic compound nanoclusters comprising Pd and Ru exhibit significantly different catalytic activity compared with their monometallic nanocluster counterparts. The catalytic activity obtained by mixing the two components is higher than that of monometallic nanoclusters of Rh, which is located between these two elements in the periodic table.[2] As illustrated by these examples, the combination with heteroelements modifies the physical and chemical properties of a metal cluster; thus, development of new functions is possible.

Thiolate-protected $Au_{25}$ cluster ($Au_{25}(SR)_{18}$)[3–20] is an extremely stable cluster and exhibits physical and chemical properties, such as photoluminescence[3,9,21], redox behavior[8], and catalytic activity[5], different from those of bulk gold. Therefore, $Au_{25}(SR)_{18}$ has attracted immense interest as a new functional nanomaterial. Elucidation of the effect of substitution with heteroatoms in this cluster is very interesting from the point of view of creating metal clusters with new physical and chemical properties on the basis of their functionalization. Previous studies have shown that substitution of a number of atoms in $Au_{25}(SR)_{18}$ with Ag and Cu results in continuous modification of the electronic structure and photoluminescence properties.[22–27] Furthermore, it has been found that the stability and reactivity of the cluster are enhanced by replacing only a single atom in $Au_{25}(SR)_{18}$ with Pt or Pd.[22,28–31]

In this study, we report on the effect of substitution in thiolate-protected trimetallic $Au_{24-n}Cu_nPd$ clusters obtained by substituting $Au_{25}(SR)_{18}$ with two kinds of heteroelements. As described above, Cu substitution of $Au_{25}(SR)_{18}$ enables continuous modification of the electronic structure of the cluster.[22] However, the same Cu substitution of $Au_{25}(SR)_{18}$ also induces instability of the cluster.[27] For synthesis of a stable cluster containing an element that induces destabilization, it is essential to provide the cluster with some kind of tool to countervail this destabilizing effect. Our previous study revealed that use of a selenolate ligand is an efficient means of achieving this.[32] Conversely, substitution of a central atom with Pd also induces high stability.[22,29,30] In the present study, with the aim of developing a means to compensate for the instability resulting from Cu substitution by replacement with a heteroatom, we prepared a mixture of $Au_{24-n}Cu_nPd(SC_{12}H_{25})_{18}$ and $Au_{25-n}Cu_n(SC_{12}H_{25})_{18}$ and compared their stability. The results revealed that in a cluster containing one Cu atom, substitution with Pd was an effective means to improve the stability of the cluster. In addition, it was also found that the presence of Pd has different effects depending on the number of Cu atoms in the cluster.

## Experimental Section

**Chemicals.** All chemicals were commercially obtained and used without further purification. Hydrogen tetrachloroaurate tetrahydrate ($HAuCl_4{\cdot}4H_2O$), palladium(II) sodium chloride trihydrate ($PdCl_2{\cdot}2NaCl{\cdot}3H_2O$), copper(II) acetylacetonate ($Cu(C_5H_7O_2)_2$), tetraoctylammonium bromide ($(C_8H_{17})_4NBr$), sodium tetrahydroborate ($NaBH_4$), 1-dodecanethiol ($C_{12}H_{25}SH$), 2-phenylethanethiol ($PhC_2H_4SH$), methanol, toluene, acetone, and acetonitrile were obtained from Wako Pure Chemical Industries. *trans*-2-[3-(4-*tert*-Butylphenyl)-2-methyl-2-propenylidene]malononitrile (DCTB) was purchased from

Santa Cruz Biotechnology. Deionized water with a resistivity of >18 MΩ cm was used.

**Synthesis.** The $Au_{24-n}Cu_nPd(SC_{12}H_{25})_{18}$ series of clusters were synthesized using a similar procedure to that used for the synthesis of $Au_{24}Pd(SC_{12}H_{25})_{18}$,[30] with slight modifications. First, a toluene solution (15 mL) of $(C_8H_{17})_4NBr$ (0.15 mmol) was added to a mixed aqueous solution of $HAuCl_4$ and $PdCl_2$·2NaCl. After stirring for 30 min, the organic phase was separated by removing the aqueous layer, and $Cu(C_5H_7O_2)_2$ was added to the separated toluene solution with a total metal concentration of metal salts ($HAuCl_4$, $PdCl_2$·2NaCl, and $Cu(C_5H_7O_2)_2$) of 0.125 mmol. The concentration ratios of $HAuCl_4$:$Cu(C_5H_7O_2)_2$:$PdCl_2$·2NaCl were set to x:y:z, where x + y + z = 25. After 10 min of stirring, $C_{12}H_{25}SH$ (1.5 mmol) was added to the toluene solution and the solution was stirred for 30 min at room temperature. The mixture was then cooled at ~0 °C in an ice bath for 30 min. An aqueous solution of $NaBH_4$ (1.25 mmol, 15 mL), cooled to ~0 °C, was then injected rapidly into this mixture under stirring at 850 rpm. After 30 min of reduction time, the reaction solution was washed with ice-cold water to remove $NaBH_4$. The organic phase was evaporated to dryness, and the product was washed with methanol to remove excess $C_{12}H_{25}SH$, $(C_8H_{17})_4NBr$, and by-products. The 25-metal atom clusters were obtained by extraction of the dried products with 10 mL of pure acetone (Figures S1–S3). For comparison purposes, $Au_{24-n}Cu_nPd(SC_2H_4Ph)_{18}$ clusters were synthesized using the same experimental conditions, except that $PhC_2H_4SH$ was used instead of $C_{12}H_{25}SH$ and that acetonitrile (10 mL) was used as the solvent for extraction.

**Characterization.** Matrix-assisted laser desorption ionization (MALDI) mass spectra were acquired on a time-of-flight mass spectrometer (JEOL Ltd., JMS-S3000) using an Nd:YAG laser (λ = 349 nm) and DCTB[33] as the MALDI matrix. The cluster-to-matrix ratio was set at 1:500, 1:1000, 1:2000, or 1:3000, and the laser fluence was reduced to the lowest value that enabled ions detection. All spectra were recorded in negative-ion mode.

Electrospray ionization (ESI) mass spectrometry was performed using a Fourier transform mass spectrometer (Bruker, Solarix). A toluene/acetonitrile solution (1 mg/mL; 1:1, v/v) of the product was electrosprayed at a flow rate of 400 μL/h.

X-ray photoelectron spectra were collected using an electron spectrometer (JEOL, JPS-9010MC) equipped with a chamber at a base pressure of ~$2\times10^{-8}$ Torr. X-rays from the Mg Kα line at 1253.6 eV were used for excitation.

Transmission electron microscopy (TEM) images were recorded on a Hitachi H-9500 electron microscope operating at 200 kV and magnification of 150,000.

UV-Visible absorption spectra of the clusters were acquired in toluene at ambient temperature on a spectrometer (JASCO, V-630). The wavelength-dependent optical data, $I$(w), were converted into energy-dependent data, $I$(E), using the following equation, which preserves the integrated spectral areas

$$I(E) = \frac{I(w)}{\left|\frac{\partial w}{\partial E}\right|} \propto I(w) \times w^2$$

**Stability against decomposition in toluene.** To investigate the stability of the clusters against decomposition in toluene, an organic synthesizer (EYELA, PPS-2510) was employed to precisely and reproducibly control the reaction temperature. Toluene solution (10 mL) containing the product (5 mg) was placed in the organic synthesizer and heated to 60 °C while stirring at 800 rpm. Before characterization, the by-products were removed from the resulting solution using a filter with pores of 200 nm.

## Calculation

Density functional theory (DFT) calculations were performed for $[Au_{23}CuPd(SCH_3)_{18}]^0$ in which one Au in the staple or in the metal core surface of $Au_{24}Pd(SC_{12}H_{25})_{18}$ is replaced with Cu. In these calculations, the experimentally synthesized clusters were modeled by replacing the dodecanethiolate with methanethiolate. Geometric optimization of the clusters was performed starting from an initial structural estimate based on $Au_{24}Pd(SCH_3)_{18}$,[30] the structure of which was optimized by DFT calculations in our previous study based on single-crystal X-ray data of $Au_{25}(SC_2H_4Ph)_{18}$.[34] This initial structure appears to be relatively symmetric; however, we did not assume a high degree of molecular symmetry in our calculations and instead performed full geometry optimization of the cluster. The TURBOMOLE package of *ab initio* quantum chemistry programs[35] was utilized in all calculations. Geometric optimizations based on a quasi-Newton–Raphson method were performed at the level of Kohn–Sham density functional theory (KS-DFT), employing the Becke three-parameter hybrid exchange functional with the Lee–Yang–Parr correlation functional (B3LYP).[36,37] The double-ζ valence quality plus polarization basis in the TURBOMOLE basis set library was adopted in the calculations, along with a 60-electron (28 electron) relativistic effective core potential[38] for the gold (palladium) atom. Optimized structures with different substitution positions of the surface of $Au_{12}Pd$ core, and the [SR–Au–SR–Au–SR–] staple were obtained at the same level of theory.

## Results and Discussion

**Characterization of the products.** Figure 1 shows the negative-ion MALDI mass spectrum of a product, which was obtained with a concentration ratio of $[HAuCl_4]$:$[Cu(C_5H_7O_2)_2]$:$[PdCl_2$·$2NaCl]$ = 23:1:1. In this mass spectrum, the peak attributable to trimetallic $Au_{23}CuPd(SC_{12}H_{25})_{18}$ can be observed in addition to those of $Au_{25-n}Cu_n(SC_{12}H_{25})_{18}$ ($n$ = 0−3) and $Au_{24}Pd(SC_{12}H_{25})_{18}$. The isotope distribution of $Au_{23}CuPd(SC_{12}H_{25})_{18}$ was in good agreement with that obtained by calculation (inset of Figure 1). In the X-ray photoelectron spectra of the product, peaks attributable to Pd (337.4 and 342.8 eV) can be observed together with those of Au (84.3 and 87.9 eV) and Cu (932.6 and 952.5 eV) (Figure S4). These results show that the product includes $Au_{23}CuPd(SC_{12}H_{25})_{18}$, which comprises three types of

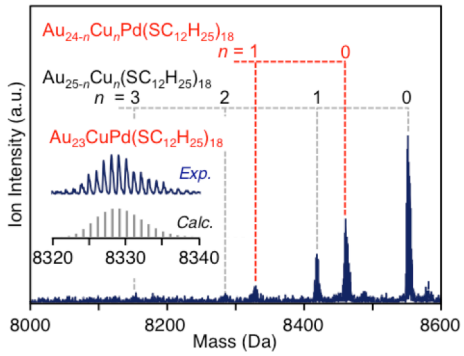


**Fig. 1** Negative-ion MALDI mass spectrum of a mixture of $Au_{24-n}Cu_nPd(SC_{12}H_{25})_{18}$ and $Au_{25-n}Cu_n(SC_{12}H_{25})_{18}$ clusters. The inset shows the calculated and experimentally determined isotope distribution of $Au_{23}CuPd(SC_{12}H_{25})_{18}$.

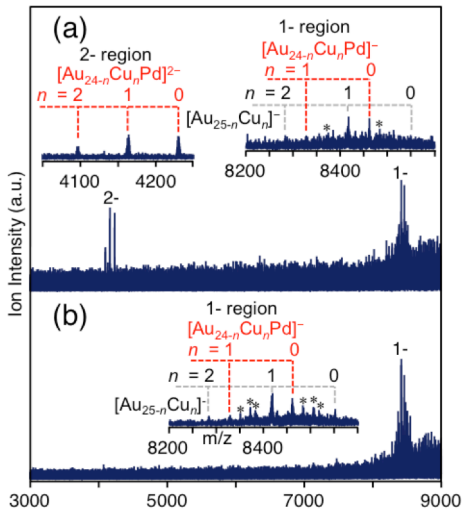


**Fig. 2** Negative-ion ESI mass spectra of a mixture of $Au_{24-n}Cu_nPd(SC_{12}H_{25})_{18}$ and $Au_{25-n}Cu_n(SC_{12}H_{25})_{18}$ clusters (a) immediately after extraction (Figure S6) and (b) after standing for 1 h in toluene at room temperature. Assignments of the peaks denoted by * are shown in Figure S5.

metal elements. To the best of our knowledge, this is the first report on the synthesis of thiolate-protected trimetallic 25-atom clusters.

To investigate the charge state of the resulting clusters, we measured the ESI mass spectra of the product. Figure 2 (a) shows the negative-ion ESI mass spectrum of the product immediately after extraction. For $Au_{25-n}Cu_n(SC_{12}H_{25})_{18}$ which does not contain Pd, a peak attributed to anion $[Au_{25-n}Cu_n(SC_{12}H_{25})_{18}]^-$ was observed (Figure S5). This is because the total number of the valence electrons satisfies the closed-shell electronic structure when $Au_{25-n}Cu_n(SC_{12}H_{25})_{18}$ are anion $[Au_{25-n}Cu_n(SC_{12}H_{25})_{18}]^-$.[39] In contrast, for $Au_{24-n}Cu_nPd(SC_{12}H_{25})_{18}$ ($n$ = 0–2) containing Pd, a peak attributable to dianion $[Au_{24-n}Cu_nPd(SC_{12}H_{25})_{18}]^{2-}$ was identified in the mass spectrum (Figure S6). Although for $Au_{24}Pd(SC_{12}H_{25})_{18}$ the total number of the valence electrons satisfies the closed-shell electronic structure when $Au_{24}Pd(SC_{12}H_{25})_{18}$ is dianion,[39]

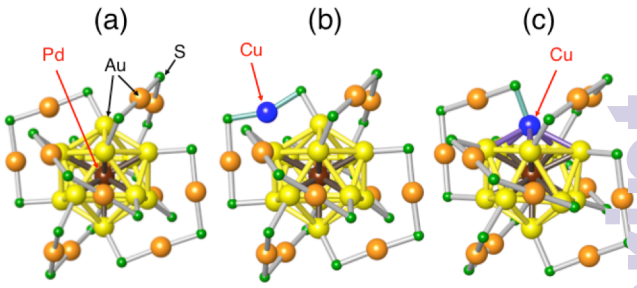


**Scheme 1** Optimized structures for (a) $[Au_{24}Pd(SCH_3)_{18}]^0$,[30] (b) $[Au_{23}CuPd(SCH_3)_{18}]^0$ in which one Au in the staple of $[Au_{24}Pd(SCH_3)_{18}]^0$ is replaced with Cu, and (c) $[Au_{23}CuPd(SCH_3)_{18}]^0$ in which one Au in the metal core surface of $[Au_{24}Pd(SCH_3)_{18}]^0$ is replaced with Cu.

in previous studies[30], it has been isolated as neutral $[Au_{24}Pd(SC_{12}H_{25})_{18}]^0$. In the present study, we measured mass spectrum immediately after extraction. Therefore, oxidation of the clusters in solution was suppressed, which could be the reason for observation of dianion $[Au_{24-n}Cu_nPd(SC_{12}H_{25})_{18}]$. These results indicate that in $Au_{24-n}Cu_nPd(SC_{12}H_{25})_{18}$ ($n$ = 0–2), immediately after extraction, dianion $[Au_{24-n}Cu_nPd(SC_{12}H_{25})_{18}]^{2-}$ is present. On the other hand, in the negative-ion ESI mass spectrum for the product after standing in toluene for 1 hour at room temperature, such dianion $[Au_{24-n}Cu_nPd(SC_{12}H_{25})_{18}]^{2-}$ were not observed and the clusters attributable to the monoanion $[Au_{24-n}Cu_nPd(SC_{12}H_{25})_{18}]$ became main species (Figure 2(b)). These results indicate that $[Au_{24-n}Cu_nPd(SC_{12}H_{25})_{18}]^{2-}$ easily undergoes oxidation and consequently becomes the monoanion $[Au_{24-n}Cu_nPd(SC_{12}H_{25})_{18}]^-$ or the neutral $[Au_{24-n}Cu_nPd(SC_{12}H_{25})_{18}]^0$ (ref. 30).

In all the $Au_{24-n}Cu_nPd(SC_{12}H_{25})_{18}$ produced in this study, only one Pd atom was included. It is therefore reasonable to consider that the synthesized $Au_{24-n}Cu_nPd(SC_{12}H_{25})_{18}$, like $Au_{24}Pd(SC_{12}H_{25})_{18}$ (Scheme 1(a)),[22,29,30] have geometrical structures in which Pd is located in the center of the metal core. That is, it can be assumed that in the structure of $Au_{24-n}Cu_nPd(SC_{12}H_{25})_{18}$, some Au atom in the staple or in the metal core surface of $Au_{24}Pd(SC_{12}H_{25})_{18}$ are replaced with Cu (Scheme 1(b)(c)). Furthermore, regarding the core-shell structured $Au_{24}Pd(SC_{12}H_{25})_{18}$, unlike other clusters that do not have this type of core-shell structure[13,33,40], the main laser dissociation product is $Au_{20}PdS_{10}$ consisting of 21 metal atoms and 10 sulfur atoms (Figure 3(a)). Also, for the $Au_{24-n}Cu_nPd(SC_{12}H_{25})_{18}$ synthesized in this study, the main laser dissociation product was $Au_{20-n}Cu_nPdS_{10}$, with the same number of metal and sulfur atoms (Figure 3(b)). These results similarly support the interpretation that $Au_{24-n}Cu_nPd(SC_{12}H_{25})_{18}$ possesses a core-shell type structure.

**Effect of trimetallization on the stability of $Au_{24-n}Cu_nPd(SC_{12}H_{25})_{18}$.** The mixture of $Au_{24-n}Cu_nPd(SC_{12}H_{25})_{18}$ ($n$ = 0,1) and $Au_{25-n}Cu_n(SC_{12}H_{25})_{18}$ ($n$ = 0–3) thus prepared was allowed to stand in a toluene at 60°C to examine the time dependence of the chemical composition of the mixture. Figure

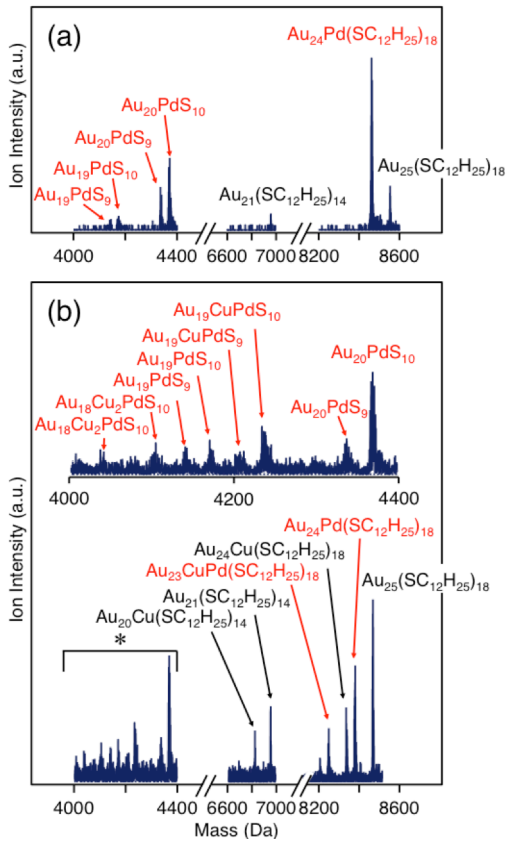


**Fig. 3** (a) Negative-ion MALDI mass spectrum of a mixture of $Au_{24}Pd(SC_{12}H_{25})_{18}$ and $Au_{25}(SC_{12}H_{25})_{18}$ observed with a fluence slightly higher than that used for the observation of non-destructive mass spectra. In (a), the $Au_{21}(SC_{12}H_{25})_{14}$-related peaks are attributed to the fragment ion from $Au_{25}(SC_{12}H_{25})_{18}$,[13,33,40] whereas the other peaks are attributed to the fragment ions from $Au_{24}Pd(SC_{12}H_{25})_{18}$.[30] (b) Negative-ion MALDI mass spectrum of a product, which was obtained with a $HAuCl_4$:$Cu(C_5H_7O_2)_2$:$PdCl_2$·2NaCl concentration ratio of 19:1:5, observed with a fluence slightly higher than that used for the observation of non-destructive mass spectra. Inset shows the detailed assignments of the asterisk-labeled peaks.

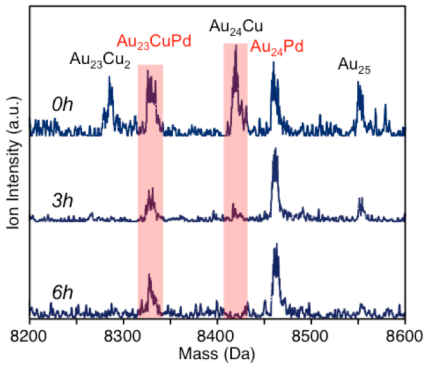


**Fig. 4** Time-dependent profiles of the chemical composition of a mixture of $Au_{24-n}Cu_nPd(SC_{12}H_{25})_{18}$ and $Au_{25-n}Cu_n(SC_{12}H_{25})_{18}$ clusters in toluene at 60 °C studied by negative-ion MALDI mass spectrometry.

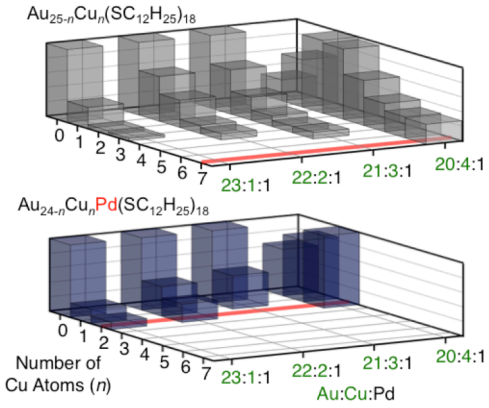


**Fig. 5** Correlation between the number of Cu atoms in the clusters and the relative ion intensity in the MALDI mass spectra for $Au_{25-n}Cu_n(SC_{12}H_{25})_{18}$ and $Au_{24-n}Cu_nPd(SC_{12}H_{25})_{18}$ synthesized with varying ratios of $[Cu(C_5H_7O_2)_2]/[HAuCl_4]$ (Figure S7). The relative ion intensities are normalized with the strongest ion peak. The red lines indicate the maximum number of the Cu atoms included in the cluster determined in a series of experiments.

4 shows the time-dependence of the MALDI mass spectra of the mixture. The relative ion intensity of $Au_{24}Cu(SC_{12}H_{25})_{18}$ compared to that of $Au_{23}CuPd(SC_{12}H_{25})_{18}$ gradually decreased with time. The main reason for this phenomenon is considered to be due to the difference in the speed of the degradation of the clusters, although we cannot exclude the possibility that the other reactions might also occur in the mixture of the clusters. Thus, Figure 4 implies that, under such severe conditions, the stability of $Au_{23}CuPd(SC_{12}H_{25})_{18}$ is higher than that of $Au_{24}Cu(SC_{12}H_{25})_{18}$. That is, as in the case of $Au_{24}Pd(SC_{12}H_{25})_{18}$,[22,29,30] Pd substitution of the central atom induces improvement in stability. The Pd−Au bond is stronger than the Au−Au bond.[41] It can be assumed that this difference in the bonding energy is the main reason for the fact that $Au_{23}CuPd(SC_{12}H_{25})_{18}$ is more stable in solution than $Au_{24}Cu(SC_{12}H_{25})_{18}$. In the case that Cu is doped in the metal core surface in $Au_{23}CuPd(SC_{12}H_{25})_{18}$ (Scheme 1(c)), the fact that Cu−Au bond is stronger than Au−Au bond[42] might also contribute to the difference in the stability between $Au_{23}CuPd(SC_{12}H_{25})_{18}$ and $Au_{24}Cu(SC_{12}H_{25})_{18}$.

On the other hand, it was also found that Pd substitution in clusters containing more Cu atoms exerts a different influence. Clusters containing more Cu atoms did not necessarily show the improved stability in solution. Furthermore, the presence of Pd in clusters containing four or more Cu atoms inhibited even the cluster formation. Figure 5 shows the correlation between the number of Cu atoms contained in clusters and the relative ion intensity in the mass spectra for $Au_{25-n}Cu_n(SC_{12}H_{25})_{18}$ and $Au_{24-n}Cu_nPd(SC_{12}H_{25})_{18}$ synthesized with various ratios of $[Cu(C_5H_7O_2)_2]/[HAuCl_4]$. As shown in Figure 5, for $Au_{25-n}Cu_n(SC_{12}H_{25})_{18}$, formation of $Au_{24-n}Cu_n(SC_{12}H_{25})_{18}$ ($n$ = 1−7) containing up to seven Cu atoms was observed. $Au_{25-n}Cu_n(SC_{12}H_{25})_{18}$ ($n$ = 6,7) have not been observed in the previous study.[27] The number of Cu atoms contained in the cluster decreases with prolonged reduction time.[43] In this study, the reduction time was shortened to 30 min (see Experiment).

**Table 1. Maximum number of Cu atoms in $Au_{25-n}Cu_n(SC_{12}H_{25})_{18}$ bimetallic clusters and $Au_{24-n}Cu_nPd(SC_{12}H_{25})_{18}$ trimetallic clusters.**

| Initial metal ion ratios Au:Cu:Pd | Maximum number of Cu atoms in $Au_{25-n}Cu_n(SC_{12}H_{25})_{18}$ | Maximum number of Cu atoms in $Au_{24-n}Cu_nPd(SC_{12}H_{25})_{18}$ |
|---|---|---|
| 23:1:1 | 3 [a] | 2 [a] |
| 22:2:1 | 4 [a] | 2 [a] |
| 21:3:1 | 5 [a] | 1 [a] |
| 20:4:1 | 7 [a] | 2 [a] |
| 22:1:2 | 3 [b] | 2 [b] |
| 21:1:3 | 0 [b] | 1 [b] |
| 20:1:4 | 3 [b] | 2 [b] |
| 19:1:5 | 3 [b] | 2 [b] |
| 18:1:6 | 3 [b] | 2 [b] |
| 17:1:7 | 3 [b] | 2 [b] |
| 21:2:2 | 3 [c] | 2 [c] |
| 20:2:3 | 6 [c] | 3 [c] |
| 19:2:4 | 3 [c] | 2 [c] |
| 18:2:5 | 5 [c] | 3 [c] |
| 17:2:6 | 4 [c] | 2 [c] |
| 20:3:2 | 4 [d] | 3 [d] |
| 18:3:4 | 4 [d] | 1 [d] |

[a] These values are from Figures 2 and S7. [b] These values are from Figure S8. [c] These values are from Figure S9. [d] These values are from Figure S10.

Section). This could be one of the reasons why $Au_{25-n}Cu_n(SC_{12}H_{25})_{18}$ ($n$ = 6,7) was observed in this study. In contrast, for $Au_{24-n}Cu_nPd(SC_{12}H_{25})_{18}$, regardless of the ratio $[Cu(C_5H_7O_2)_2]/[HAuCl_4]$, no significant formation of $Au_{24-n}Cu_nPd(SC_{12}H_{25})_{18}$ ($n \geq 4$) containing four or more Cu atoms was observed (Figures 5 and S7 and Table 1). We further attempted cluster synthesis under different conditions by increasing the relative amount of the Pd salt (the $[PdCl_2{\cdot}2NaCl]/[HAuCl_4]$ ratio); however, formation of $Au_{24-n}Cu_nPd(SC_{12}H_{25})_{18}$ ($n \geq 4$) could still not be confirmed (Figures 6(a)−(c) and S8−10 and Table 1). These results demonstrate that it is more difficult to generate $Au_{24-n}Cu_nPd(SC_{12}H_{25})_{18}$ ($n \geq 4$) than $Au_{25-n}Cu_n(SC_{12}H_{25})_{18}$ ($n \geq 4$). Similar results were obtained using phenylethanethiolate as the ligand (Figures S11−14 and Table S1). These results indicate that the presence of Pd in clusters containing four or more Cu atoms strongly inhibits cluster formation.

**Origin of instability of $Au_{24-n}Cu_nPd(SC_{12}H_{25})_{18}$ ($n \geq 4$).** The previous X-ray absorption spectroscopy on $Au_{25-n}Cu_n(SR)_{18}$ ($n \sim 1.4$) have revealed that Cu substitution occurs at Au in the staple.[44] Furthermore, it has been revealed by density functional theory (DFT) calculations[27,45] that a large strain is generated in the framework structure of the such Cu-substituted cluster.[27] It is presumed that such strain in the framework structure is one of the factors causing $Au_{25-n}Cu_n(SC_{12}H_{25})_{18}$ to disappear readily in solution.[27] Then, we studied the geometrical structure of $Au_{23}CuPd(SCH_3)_{18}$ in which one Au atom in the staple is replaced with Cu (Scheme 1(b)) by DFT calculation. Figure 7 shows histograms of the intermetallic bond length in the optimized structure for

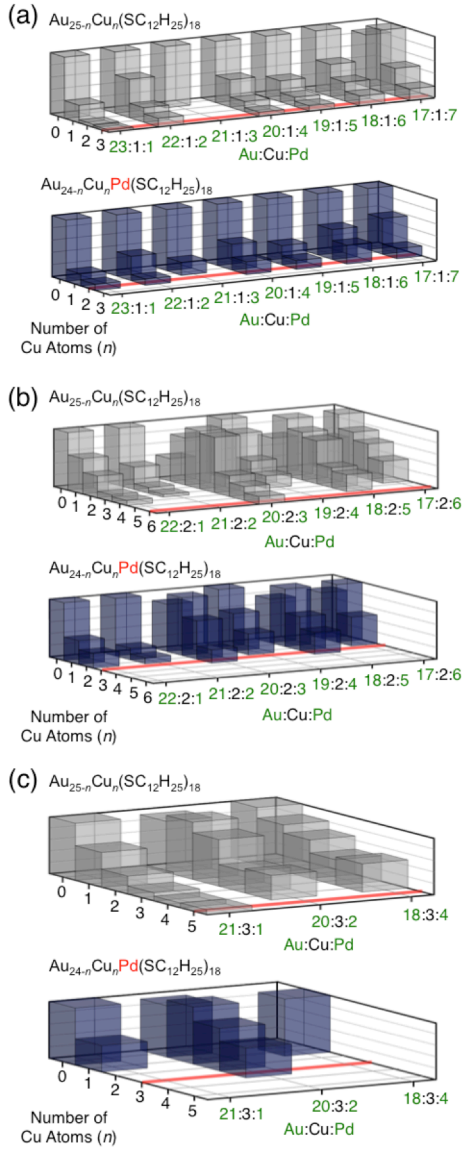


**Fig. 6** Correlation between the number of Cu atoms in clusters and the relative ion intensity in the mass spectra for $Au_{25-n}Cu_n(SC_{12}H_{25})_{18}$ and $Au_{24-n}Cu_nPd(SC_{12}H_{25})_{18}$ synthesized with various ratios of $[PdCl_2{\cdot}2NaCl]:[HAuCl_4]$. The ratio of $[Cu(C_5H_7O_2)_2]$ was fixed such that $[HAuCl_4]:[Cu(C_5H_7O_2)_2]:[PdCl_2{\cdot}2NaCl]$ was (a) $x$:1:$z$, where $x + z = 24$ (Figure S8), (b) $x$:2:$z$, where $x + z = 23$ (Figure S9), or (c) $x$:3:$z$, where $x + z = 22$ (Figure S10). The red lines indicate the maximum number of the Cu atoms present in a cluster determined in a series of experiments.

$[Au_{25}(SCH_3)]^-$, $[Au_{24}Cu(SCH_3)]^-$, $[Au_{24}Pd(SCH_3)]^0$, and $[Au_{23}CuPd(SCH_3)]^0$. As shown in Figure 7, the intermetallic bond lengths of $[Au_{24}Pd(SCH_3)]^0$ and $[Au_{23}CuPd(SCH_3)]^0$ are longer than those of $[Au_{25}(SCH_3)]^-$ and $[Au_{24}Cu(SCH_3)]^-$. Furthermore, the dispersion of data also increases in $[Au_{24}Pd(SCH_3)]^0$ and $[Au_{23}CuPd(SCH_3)]^0$ than $[Au_{25}(SCH_3)]^-$ and $[Au_{24}Cu(SCH_3)]^-$. These results indicate that Pd substitution induces an even larger strain in the framework structure than Cu substitution. In $Au_{24-n}Cu_nPd(SC_{12}H_{25})_{18}$ ($n \geq 4$) containing four or more Cu atoms, comparatively large strain of the framework structure can be expected. Regarding

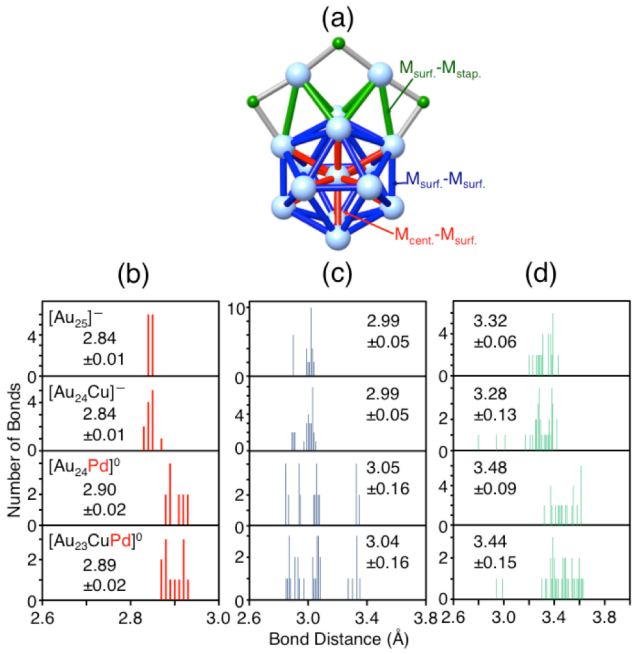


**Fig. 7** (a) Anatomy of 25 metal atom cluster highlighting three kinds of bond. (b)−(d) Histograms of the intermetallic bond length in $[Au_{25}(SCH_3)]^-$, $[Au_{24}Cu(SCH_3)]^-$, $[Au_{24}Pd(SCH_3)]^0$, and $[Au_{23}CuPd(SCH_3)]^0$ in which one Au atom in the staple is replaced with Cu (Scheme 1(b)); (b) $M_{cent.}$−$M_{surf.}$, (c) $M_{surf.}$−$M_{surf.}$ and (d) $M_{surf.}$−$M_{stap.}$.

the site of Cu substitution, the possibility of substitution in the surface of metal core (Scheme 1(c)) cannot be excluded (Table S2); however, even when Cu substitution occurs in the metal core surface, the same distortion in the geometrical structure was manifested (Figure S15). It is presumed that such strain in geometrical structure inhibits cluster formation for $Au_{24-n}Cu_nPd(SC_{12}H_{25})_{18}$ ($n \geq 4$).

## Conclusions

In the present study, we synthesized $Au_{24-n}Cu_nPd(SC_{12}H_{25})_{18}$ clusters, including three types of metal elements, and examined the effect of Pd substitution in these clusters. We found that in an $Au_{23}CuPd(SC_{12}H_{25})_{18}$, the presence of Pd enhanced the stability of the clusters. Conversely, in this type of trimetallic system, different effects will be apparent depending on the number of Cu atoms contained, and for clusters containing four or more Cu atoms, it was determined that even cluster formation was inhibited. Elucidation of the effect of substitution with heteroatoms in $Au_{25}(SR)_{18}$ will hopefully lead to the establishment of means for creating metal clusters with high functionality. The findings of this study are also expected to provide guidelines for imparting new physical and chemical properties to $Au_{25}(SR)_{18}$ clusters.

## Acknowledgements

We thank Dr. Yoshiki Niihori for his valuable comments. The ESI-MS analysis was supported by the Collaborative Research Program of the Institute for Chemical Research, Kyoto University. This work was financially supported by a Grants-in-Aid for Scientific Research (Nos. 25288009, 25102539 and 26620016), the Canon Foundation, and the Iketani Science and Technology Foundation.

## Notes and references

[a] *Department of Applied Chemistry, Faculty of Science, Tokyo University of Science, 1-3 Kagurazaka, Shinjuku-ku, Tokyo 162−8601, Japan. Fax: +81−3−5261−4631; Tel: +81−3−5228−9145; E-mail: negishi@rs.kagu.tus.ac.jp*
[b] *Department of Theoretical and Computational Molecular Science, Institute for Molecular Science, Myodaiji, Okazaki, Aichi 444−8585, Japan.*
[c] *Elements Strategy Initiative for Catalysts and Batteries (ESICB), Kyoto University, Katsura, Kyoto 615−8520, Japan.*
[d] *Department of Materials Molecular Science, Institute for Molecular Science, Myodaiji, Okazaki, Aichi 444−8585, Japan.*
[e] *Photocatalysis International Research Center, Tokyo University of Science, 2641 Yamazaki, Noda, Chiba 278−8510, Japan.*
† Electronic Supplementary Information (ESI) available: Details of product characterization data. See DOI: 10.1039/b000000x/

1 H. Zhang, T. Watanabe, M. Okumura, M. Haruta and N. Toshima, *Nat. Mater.*, 2012, **11**, 49–52.
2 K. Kusada, H. Kobayashi, R. Ikeda, Y. Kubota, M. Takata, S. Toh, T. Yamamoto, S. Matsumura, N. Sumi, K. Sato, K. Nagaoka and H. Kitagawa, *J. Am. Chem. Soc.*, 2014, **136**, 1864–1871.
3 Y. Negishi, K. Nobusada and T. Tsukuda, *J. Am. Chem. Soc.*, 2005, **127**, 5261–5270.
4 T. Tsukuda, *Bull. Chem. Soc. Jpn.*, 2012, **85**, 151–168.
5 G. Li and R. Jin, *Acc. Chem. Res.*, 2013, **46**, 1749–1758.
6 Z. Luo, V. Nachammai, B. Zhang, N. Yan, D. T. Leong, D.-e. Jiang and J. Xie, *J. Am. Chem. Soc.*, 2014, **136**, 10577–10580.
7 A. C. Dharmaratne, T. Krick and A. Dass, *J. Am. Chem. Soc.*, 2009, **131**, 13604–13605.
8 J. F. Parker, C. A. Fields-Zinna and R. W. Murray, *Acc. Chem. Res.*, 2010, **43**, 1289–1296.
9 E. S. Shibu, M. A. H. Muhammed, T. Tsukuda and T. Pradeep, *J. Phys. Chem. C*, 2008, **112**, 12168–12176.
10 T. W. Ni, M. A. Tofanelli, B. D. Phillips and C. J. Ackerson, *Inorg. Chem.*, 2014, **53**, 6500–6502.
11 T. Dainese, S. Antonello, J. A. Gascón, F. Pan, N. V. Perera, M. Ruzzi, A. Venzo, A. Zoleo, K. Rissanen and F. Maran, *ACS Nano*, 2014, **8**, 3904–3912.
12 D.-e. Jiang, M. Kühn, Q. Tang and F. Weigend, *J. Phys. Chem. Lett.*, 2014, **5**, 3286–3289.
13 C. Liu, S. Lin, Y. Pei and X. C. Zeng, *J. Am. Chem. Soc.*, 2013, **135**, 18067–18079.
14 A. Tlahuice-Flores, R. L. Whetten and M. Jose-Yacaman, *J. Phys. Chem. C*, 2013, **117,** 20867–20875.
15 P. Zhang, *J. Phys. Chem. C*, 2014, **118**, 25291–25299.
16 H. Chong, P. Li, S. Wang, F. Fu, J. Xiang, M. Zhu and Y. Li, *Sci. Rep.*, 2013, **3**, 3214.
17 K. Kwak, S. S. Kumar, K. Pyo and D. Lee, *ACS Nano*, 2014, **8**, 671–679.
18 Z. Wu, D.-e. Jiang, A. K. P. Mann, D. R. Mullins, Z.-A. Qian, L. F. Allard, C. Zeng, R. Jin and S. H. Overbury, *J. Am. Chem. Soc.*, 2014, **136**, 6111–6122.
19 K. G. Stamplecoskie and P. V. Kamat, *J. Am. Chem. Soc.*, 2014, **136**, 11093–11099.
20 Y. Negishi, *Bull. Chem. Soc. Jpn.*, 2014, **87**, 375–389.
21 S. Link, A. Beeby, S. FitzGerald, M. A. El-Sayed, T. G. Schaaff and R. L. Whetten, *J. Phys. Chem. B*, 2002, **106**, 3410–3415.
22 Y. Negishi, W. Kurashige, Y. Niihori and K. Nobusada, *Phys. Chem. Chem. Phys.*, 2013, **15**, 18736–18751.
23 Y. Negishi, T. Iwai and M. Ide, *Chem. Commun.*, 2010, **46**, 4713–4715.
24 R. Jin and K. Nobusada, *Nano Res.* 2014, **7**, 285–300.

25 E. B. Guidez, V. Mäkinen, H. Häkkinen and C. M. Aikens, *J. Phys. Chem. C*, 2012, **116**, 20617–20624.
26 D. R. Kauffman, D. Alfonso, C. Matranga, H. Qian and R. Jin, *J. Phys. Chem. C*, 2013, **117**, 7914–7923.
27 Y. Negishi, K. Munakata, W. Ohgake and K. Nobusada, *J. Phys. Chem. Lett.*, 2012, **3**, 2209–2214.
28 H. Qian, D.-e. Jiang, G. Li, C. Gayathri, A. Das, R. R. Gil and R. Jin, *J. Am. Chem. Soc.*, 2012, **134**, 16159–16162.
29 W. Kurashige, Y. Niihori, S. Sharma and Y. Negishi, *J. Phys. Chem. Lett.*, 2014, **5**, 4134–4142.
30 Y. Negishi, W. Kurashige, Y. Niihori, T. Iwasa and K. Nobusada, *Phys. Chem. Chem. Phys.*, 2010, **12**, 6219–6225.
31 Y. Niihori, W. Kurashige, M. Matsuzaki and Y. Negishi, *Nanoscale*, 2013, **5**, 508–512.
32 W. Kurashige, K. Munakata, K. Nobusada and Y. Negishi, *Chem. Commun.*, 2013, **49**, 5447–5449.
33 A. Dass, A. Stevenson, G. R. Dubay, J. B. Tracy and R. W. Murray, *J. Am. Chem. Soc.*, 2008, **130**, 5940–5946.
34 M. W. Heaven, A. Dass, P. S. White, K. M. Holt and R. W. Murray, *J. Am. Chem. Soc.*, 2008, **130**, 3754–3755.
35 *TURBOMOLE*, version 6.3, TURBOMOLE GmbH, Karlsruhe, Germany.
36 C. Lee, W. Yang and R. G. Parr, *Phys. Rev. B*, 1988, **37**, 785–789.
37 A. D. Becke, *J. Chem. Phys.*, 1993, **98**, 5648–5652.
38 D. Andrae, U. Häuβermann, M. Dolg, H. Stoll and H. Preuβ, *Theor. Chim. Acta*, 1990, **77**, 123–141.
39 M. Walter, J. Akola, O. Lopez-Acevedo, P. D. Jadzinsky, G. Calero, C. J. Ackerson, R. L. Whetten, H. Grönbeck and H. Häkkinen, *Proc. Natl. Acad. Sci. U.S.A.*, 2008, **105**, 9157–9162.
40 O. Lopez-Acevedo and H. Häkkinen, *Eur. Phys. J. D*, 2011, **63**, 311–314.
41 D. Yuan, X. Gong and R. Wu, *Phys. Rev. B*, 2007, **75**, 085428.
42 C. W. Bauschlicher, Jr., S. R. Langhoff and H. Partridge, *J. Chem. Phys.*, 1989, **91**, 2412–2419.
43 E. Gottlieb, H. Qian and R. Jin, *Chem. Eur. J.*, 2013, **19**, 4238–4243.
44 S. Yamazoe, W. Kurashige, K. Nobusada, Y. Negishi, T. Tsukuda, *J. Phys. Chem. C*, 2014, **118**, 25284–25290.
45 M. J. Hartmann, H. Häkkinen, J. E. Millstone and D. S. Lambrecht, *J. Phys. Chem. C*, DOI: 10.1021/jp5125475.